# **Engineering the Internal Structure of Hollow Nanostructures for Enhanced Plasmonic Properties**

Shikuan Shao† and Xiaohu Xia†,‡,\*

†Department of Chemistry, University of Central Florida, Orlando, Florida 32816, United States;

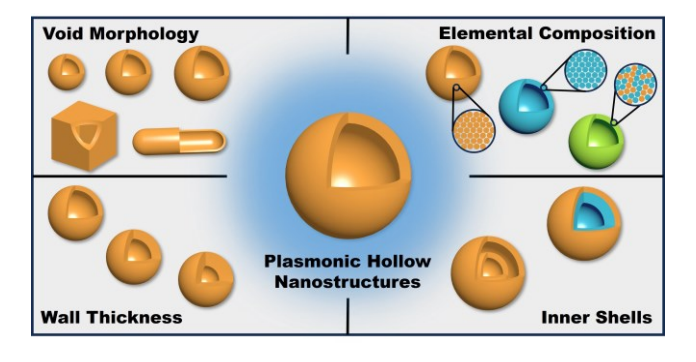
<sup>‡</sup>NanoScience Technology Center, University of Central Florida, Orlando, Florida 32816, United States.

<sup>\*</sup>Corresponding author. E-mail: Xiaohu.Xia@ucf.edu

#### Abstract

Plasmonic nanostructures with hollow interiors have emerged as a class of multifunctional materials for many applications, owing to their superior plasmonic activities relative to their solid counterparts. Besides outer surfaces, hollow nanostructures also have inner surfaces, which facilitate the control of internal structures. In this Perspective, we discuss recent progress in engineering the internal structure of hollow nanostructures for enhanced plasmonic properties. We start with a brief introduction to the synthetic methods that can effectively control the internal structure of hollow nanostructures. We then elaborate on the impact of each parameter of internal structure on plasmonic properties, where how to rationally design and experimentally control these parameters is also discussed. Afterwards, we highlight the applications of plasmonic hollow nanostructures with well-controlled internal structures in biosensing and photocatalysis. Lastly, we conclude this perspective with the challenges and opportunities in this emerging field.

**TOC Graphic** 



#### 1. INTRODUCTION

Over the past couple of decades, design, synthesis, and utilization of hollow nanostructures with tailored plasmonic properties have emerged as a frontier of nano research and innovation. Plasmonic hollow nanostructures (PHNs) have demonstrated remarkable potential across diverse applications ranging from sensing, 1,2 biomedicine, 3-10 electronics, 11 imaging, 12,13 catalysis, 14 and energy harvesting. 15 One of the primary factors contributing to the superior plasmonic performance of PHNs lies in a mechanism called "plasmon hybridization", 16-20 which involves intricate interaction and merging of the localized and delocalized surface plasmons within their hollow interiors. As a result, the "hybridized" plasmons of the hollow nanostructures shift to a lower energy level and couple more strongly with the optical field, resulting in significantly enhanced and more homogeneously distributed localized surface plasmon resonance (LSPR). 21-24 In addition to their outstanding plasmonic activities, PHNs possess unique physicochemical properties such as large surface-to-volume ratios and highly open structures. 25-30

The design and fabrication of hollow nanostructures with desired plasmonic properties typically rely on the controls over both internal and external morphological and structural parameters, such as shape, size, elemental composition, wall thickness, and degree of hollowness.<sup>25,31-37</sup> These controls can be achieved chemically by a myriad of synthetic methods developed over the years. Specifically, the synthetic methods can be broadly divided into two categories: i) template-based methods, which involve the coating of a prefabricated template (hard or soft) with a layer of shell material, followed by removal of the template. A representative example of this method is galvanic replacement reaction (GRR), 25,38-42 which will be emphasized in the following discussion; and ii) template-free methods, which rely on the intrinsic properties of precursor materials and reaction conditions to spontaneously generate the desired nanostructures in a chemical synthesis. Examples include those based on self-assembly, <sup>43</sup> Ostwald ripening, <sup>44-46</sup> and self-deformation. <sup>47-49</sup> Thanks to the efforts by many research groups, a diverse array of PHNs (e.g., nanoboxes, <sup>27,50</sup> nanocages, <sup>1,2,51-53</sup> nanoshells, <sup>54-56</sup> nanostars, <sup>57,58</sup> and nanoframes <sup>59-64</sup>) have been reported over the past few decades. These hollow nanostructures are tailored with unique plasmonic properties that can be utilized in many technologically important applications, especially in the areas of biomedicine and photocatalysis. <sup>29,39,65-73</sup>

This article discusses recent endeavors dedicated to engineering the internal structure of PHNs with an emphasis on those prepared *via* GRR-based synthetic methods. In this paper, the

"internal structure" refers to the morphology and composition inside the outer surface layer of a PHN. We begin with a brief introduction to the synthetic methodologies for PHNs with controlled internal structures. We then elaborate on how to rationally design the internal structure of a PHN by detailing the impacts of several key parameters of internal structure, including the morphology of hollow interior (or void), elemental composition of walls, wall thickness, and inner shells. Later, a few recent applications of PHNs in biosensing and photocatalysis are highlighted. Finally, an overview and perspectives on the current and future research are provided, where the challenges and opportunities in this niche field are discussed.

#### 2. SYNTHETIC METHODOLOGIES

Conventionally, PHNs are synthesized by straightforward hard-template methods. Typically, desired materials are deposited onto hard templates with functionalized surfaces, followed by selective removal of the templates *via* dissolution, thermal decomposition, chemical etching, or calcination.<sup>31</sup> Despite the conceptual simplicity of the process, this conventional method has several intrinsic limitations. Obstacles include the simple configurations of final products, tedious surface modification procedures of the templates, and the utilization of toxic etchants and solvents during the template removal process,<sup>26</sup> which greatly restrict the broad application of this method. Therefore, developing self-template<sup>47,74</sup> or template-free methods based on one or combined mechanisms is of great significance. In the following discussion, we highlight the galvanic replacement reaction (GRR)-based synthetic methods, which are powerful for controlling the internal structure of a PHN. Those non-GRR-based synthetic methods will also be briefly discussed.

#### 2.1. GRR-Based Synthetic Methods

Galvanic replacement reaction (GRR) is a redox process driven by the reduction potential difference between reactants (usually two metals). <sup>39,40</sup> In a conventional GRR-based synthesis of PHNs (Figure 1a), the nanocrystal of metal A, acting as the sacrificial template, is hollowed out by the ions of metal B with a higher reduction potential in solution phase through the process: y/x  $A_{(s)} + B^{y+}_{(aq)} \rightarrow y/x$   $A^{x+}_{(aq)} + B_{(s)}$ . The complete dissolution of metal A template eventually resulted in the formation of a nanostructure featuring a hollow interior as well as a porous A-B alloyed wall as the final product. Details about conventional GRR-based methods can be found in our previously published review. <sup>25</sup> In the following discussion, we highlight those innovative synthetic

approaches based on conventional GRR, which can effectively control the internal structure of PHNs.

GRR be combined with the co-reduction mechanism by adding a mild reducing agent (e.g., formaldehyde, sodium citrate, and ascorbic acid) during the reaction. T5-77 As a result, competition arises between the reduction of metal ions  $B^{y+}$  by sacrificial template A and by this reducing agent (Figure 1b). Meanwhile, the newly oxidized ions  $A^{x+}$  from the sacrificial template are reduced back to the nanostructures by the reducing agent. This complex process provides new pathways for tuning the wall thickness of a PHN over a wider range compared with conventional GRR-based method. For example, in a recent work by Ye et al., Ag-Au nanoshells with a wall thickness of  $\sim$ 15 nm were synthesized by adding sodium citrate as a reducing agent. The extinction intensity of the Ag-Au nanoshells was four times higher than that of Ag-Au nanocages prepared by conventional GRR.

Another innovative approach that has been recently developed was to couple GRR with the template regeneration process (see Figure 1c).<sup>1,2</sup> Specifically, during the course of template regeneration, metal A selectively grows into the void of an A-B alloyed hollow nanostructure prepared by conventional GRR, forming an A@A-B shell@shell nanostructure (or core@shell structure when the void is fully stuffed with metal A atoms). The key to ensuring the selective deposition of adatoms on the inner surface of hollow nanostructure is to lower the deposition rate of metal A atoms, allowing them enough time to migrate from the outer surface to the inner surface. This process is inherently driven by thermodynamics since the growth of metal A on the inner surface of a hollow nanostructure reduces its surface area and thereby minimizes the system total free energy.<sup>78</sup> It is worth mentioning that, in addition to the controlling of the deposition and surface diffusion rates, lattice mismatch also plays an important role in this process. Specifically, the distribution of metals A and B in the wall of hollow nanostructure prepared by GRR is inhomogeneous, typically consisting of a metal B-rich outer surface and a metal A-rich inner surface. The newly generated metal A atoms during the growth tend to selectively deposit on the metal A-rich inner surface because there is no lattice mismatch in forming an A-A bond, which further promotes the formation of A@A-B shell@shell nanostructure as the final product. More detailed discussions about the mechanism of template regeneration can be found in our previous publications.  $^{1,2,78-80}$  Remarkably, the resultant A@A-B structure can serve as a regenerated template for a new round of galvanic replacement. Repeating such sequential processes of template

regeneration and galvanic replacement enables the synthesis of highly diverse hollow structures with tunable wall thickness and elemental compositions (e.g., by introducing a third metal C), regardless of the stoichiometry imposed by the galvanic reactions. In a recent work by our group,<sup>2</sup> metallic nanocages with highly tunable wall thickness and controlled elemental compositions were successfully prepared by this method.

In addition to co-reduction and template regeneration, GRR can be combined with a physical process called the Kirkendall effect. This approach can effectively control the void structure inside a hollow nanostructure by utilizing the unbalanced interdiffusion rates between the metals involved in the system. Moreover, a chemical potential regulating mechanism can also be integrated to GRR. By modifying both the template surface and the metal salt precursor with different chemical ligands to form metal-ligand coordination complexes, it is possible to manipulate the reduction potential that is the inherent driving force of GRR. As a result, the product of this surface-limited reaction can be either a core-shell nanostructure or a pure alloyed-shell nanostructure freely.

These versatile approaches based on GRR have been demonstrated to be effective in controlling the physicochemical parameters of hollow nanostructures, especially their internal structures. As the requirements by various applications become increasingly sophisticated and challenging, development of new synthetic approaches for finely crafting hollow nanostructures remains a promising direction of fundamental research.

## 2.2. Non-GRR-Based Synthetic Methods

In addition to GRR-based methods, self-assembly and soft-template strategies are sometimes applied to fabricate hollow nanostructures. Specifically, pre-synthesized nanoparticles, as building blocks, are self-organized or deposited onto a surfactant-decorated template, forming desired architectures through various weak interactions. The resultant hollow structures are typically in the form of vesicles, of which size and wall thickness can be controlled by adjusting the size, concentration, surface ligand, and/or composition of pre-synthesized nanoparticles. For example, in a work by He et al., Au nanoparticles (Au NPs) modified with amphiphilic block copolymers were assembled to form vesicles with hollow interiors. The morphology of the hollow interior had strong dependences on length of polymer tethers and the size of Au NPs. In another work by Niikura et al., Au vesicles were prepared by assembling semifluorinated oligo(ethylene

glycol) ligand-coated Au NPs. The diameter and void size of the vesicles can be tuned by altering the size of Au NPs. For instance, the utilization of 5 nm and 10 nm Au NPs resulted in the formation of vesicles with average diameters of 60 and 95 nm, respectively. Recent studies have indicated that the LSPR peaks of these vesicles are mostly located at long wavelengths, close to or within the near-infrared (NIR) region. It is worth mentioning that these self-assembly strategies may face some potential issues for applications. For instance, the self-assembly process usually requires multiple steps of chemical functionalization and thus is difficult to scale up the synthesis. In addition, the synthetic methods provide limited control over the uniformity and degree of aggregation of the products. Moreover, the synthesized hollow structures sometimes lack outstanding chemical and thermal stabilities, making it not straightforward to use them for certain applications.

#### 3. IMPACT OF INTERNAL STRUCTURE ON PLASMONIC PROPERTY

The plasmonic properties of PHNs have a strong dependence on their internal structure. In this section, we discuss the impact of various parameters of internal structure. In the following discussions, "void" refers to the hollow interior of a PHN. "wall" refers to the layer of materials between the inner and outer surfaces of a PHN. "inner shell" is defined as the shell close to the inner surfaces of a PHN that are separated from the most outer shell by a gap or an interface.

## 3.1. Impact of Void Morphology

The morphology, including both size and shape, of void has a direct impact on the plasmonic properties of PHNs. It is worth noting that, for PHNs prepared by GRR-based methods, the morphology of void normally resembles that of the initial template. In general, for PHNs of similar void shapes and comparable wall thicknesses, increasing void size leads to redshift of the major LSPR peaks. For PHNs of similar void sizes, reducing the symmetry of void shape also results in redshift of major LSPR peaks. In some cases, in addition to redshift of major LSPR peaks, new shoulder peaks may emerge due to the electron restoring force energy and polarizability.<sup>23,91</sup>

By controlling the void morphology, major LSPR peaks of PHNs can be tuned in a wide range, spanning from the visible light to the deep NIR window. Particularly, for *in vivo* biological applications such as photothermal therapy and biomedical imaging, nano-agents with NIR absorption are preferred since the light in this window provides deeper tissue penetration ability,

higher maximum permission exposure (MPE) value, lower autofluorescence background, and reduced photo scattering. 92-96 Increasing the void size represents an effective approach to tuning the LSPR peak of PHN. For example, in a recent study, our group synthesized a series of Ag-Au nanocages that had the same void shape (i.e., cubic shape) but different void sizes ranging from ~ 27 nm to 113 nm (Figure 2a-c). As shown by Figure 2d, the major LSPR peaks of these nanocages red shifted from 680 to 790 nm as the void size increased. In this approach of void size control, PHNs are enlarged as the void size is increased. Therefore, this approach is often limited by the maximum size suitable for certain applications. As an alternative approach, controlling the shape of void can effectively tune the LSPR peak of PHNs without necessarily increasing particle size. Especially, LSPR peak red shifts as the symmetry of void shape is reduced. For instance, in a work by Cai et al.<sup>97</sup> (see Figure 2e,f), gold hollow nanorods were synthesized through the galvanic replacement reaction between selenium-doped tellurium nanorods as sacrificial templates and Au<sup>3+</sup>. The hollow nanorods with an aspect ratio of 3.0 have a longitudinal LSPR peak at ~1000 nm along with a transverse LSPR peak at ~600 nm. They were demonstrated to exhibit excellent optical and photothermal performance and could be used as a multifunctional platform for the diagnosis and treatment of cancer.

## 3.2. Impact of Elemental Composition of Walls

The elemental composition of walls of PHNs directly affects their interaction with light, resulting in different plasmonic properties (*e.g.*, position and width of the resonance peak). In general, Ag, Au, and Cu are the three dominant plasmonically active metals owing to their intrinsic permittivity.<sup>21</sup> In the case of PHNs prepared by GRR-based methods, the elemental composition usually exists in the form of alloys, which offer a greater tunability over mono-metallic PHNs.<sup>98</sup>

A variety of elemental combinations have been utilized in PHNs, of which Ag-Au is one of the most commonly used systems. 52,99-101 This could be attributed to the following merits: *i*) Superior extinction intensity and tunability. Ag and Au are capable of generating plasmon resonance from the visible to NIR range and possess the highest two plasmonic quality factors (Q-factor); 102-104 *ii*) Outstanding chemical and thermal stabilities. Ag and Au as noble metals are relatively chemically inert, especially when they form alloys; 105 *iii*) Good biocompatibility. Ag-Au PHNs can be well dispersed in aqueous solutions with bio-friendly ligands serving as stabilizers (*e.g.*, citrate and ascorbic acid). Ag and Au also enable simple and efficient surface modifications

with biomolecules (e.g., antibodies, peptides, and nucleic acids) by means of electrostatic interactions and/or thiol-gold/silver chemistry. 106-108

To design the elemental composition of PHNs for specific applications, a few other important factors, in addition to their plasmonic properties, need to be considered. For example, to reduce the materials cost of PHNs, inexpensive non-noble metals such as Al, Ni, Fe, and Co can be incorporated into the PHNs. 98,109 For instance, in a work by Lindley et al., 110 Co<sub>2</sub>B nanoparticles are used as sacrificial templates for galvanic replacement reactions with HAuCl<sub>4</sub>. The resultant Co<sub>2</sub>B-Au nanoshells displayed outstanding plasmonic properties, including highly tunable LSPR peaks. Significantly, materials cost of the Co<sub>2</sub>B-Au nanoshells was lower than nanoshells of pure Au due to the utilization of less expensive cobalt and boron. Besides using metallic templates, PHNs can also be prepared by using non-metal templates. For instance, the Se-Au hollow nanoparticles formed through the GRR between Se template and Au<sup>3+</sup> ions have been demonstrated to be highly suitable for *in vivo* tumor imaging and therapeutic applications because of their excellent biocompatibility and the antitumor activity of Selenium. 10,97,111-113

## 3.3. Impact of Wall Thickness

Wall thickness has been demonstrated to be a key parameter in influencing the plasmonic properties of PHNs. Despite observations from many case studies, it has been challenging to systematically investigate the explicit role played by wall thickness in determining the plasmonic properties of PHNs in experiments. This is mainly because the change of wall thickness is often accompanied by the alternations of void size and/or outer diameter of a PHN, two other parameters that also influence the plasmonic properties.

With the recent advancement of nano-synthesis, it has become feasible to specifically control wall thickness of PHNs, making it possible to single out the role played by wall thickness. In a recent study, our group designed two complementary sets of experiments using Ag-Au nanocage as a model system. In the first set of experiments, we fixed the internal void size of the nanocages and altered the wall thickness by depositing Ag-Au on the outer surfaces of the cages. These cages are termed "[Ag-Au] $_{0-n}$  cages" (O: wall thickness increases toward outer surfaces; n: number of consecutive Ag-Au layers that are correlated to wall thickness, n = 1-5, see

Figure 3a). In another set of experiments, we fixed the outer diameter of the nanocages and changed the wall thickness by depositing Ag-Au on the inner surfaces of the cages. These cages are termed "[Ag-Au]<sub>I-n</sub> cages" (I: wall thickness increases toward inner surfaces; n: number of consecutive Ag-Au layers, n = 1-5, see Figure 3b). We found that as the wall thickness increases, the LSPR peaks of both sets of nanocages tend to shift to shorter wavelengths (*i.e.*, blueshift), which is accompanied by the decrease of bandwidth (Figure 3c,d). Notably, the decrease in the bandwidth of [Ag-Au]<sub>I-n</sub> cages is much more evident than the case of [Ag-Au]<sub>O-n</sub> cages. Interestingly, we also found that the major LSPR absorption  $\lambda_{\text{max}}$  and the outer size to wall thickness ratio (L/t) of both sets of nanocages are linearly correlated. Additionally, the impact of wall thickness on the extinction intensities of both sets of nanocages was also studied. For the [Ag-Au]<sub>O-n</sub> cages, their extinction intensities increased dramatically with the increase in wall thickness. For the [Ag-Au]<sub>I-n</sub> cages, the differences in their extinction intensities are less significant. Collectively, the extinction intensities of the Ag-Au nanocages are affected by both wall thickness and void size, where the wall thickness plays a dominant role.

It should be pointed out that wall thickness not only affects plasmonic properties of PHNs but also influences their thermal stabilities. In many applications, thermal stability of a PHN needs to be carefully considered. For example, outstanding thermal stability of PHNs is desired in laser-based applications, where the localized temperature of a PHN may reach a level as high as several hundred Celsius. <sup>115-117</sup> In a case study, we found the thermal stability of Ag-Au nanocages could be efficiently enhanced by thickening their walls. <sup>118</sup> Further studies on other PHN systems deserve thorough examinations in the future.

## 3.4. Impact of Inner Shells

PHNs having one or multiple inner shells are a class of nanostructures featuring unique plasmonic properties. Generally, they can be broadly classified into two categories: *i*) PHNs with inner shells that are segregated from the most outer shell by gaps in between them (referred to as "segregated inner shells"); and *ii*) PHNs with inner shells that are consecutively attached to the most outer shell without gaps (referred to as "integrated inner shells"), where an interface is formed between the materials of outer and inner shells.

PHNs with segregated inner shells, also known as "nano-matryoshka", have been prepared with a variety of shapes (e.g., nanorattles, nanoshells, nanoboxes, nanotubes, and

nanoframes<sup>60,61,119-121</sup>) since they were first reported by Sun et al.<sup>122</sup> The synthetic method of the nano-matryoshka (which is typically GRR-based) involves epitaxially growing a metal as the template on a pre-formed nanoshell, and then growing another layer of shell and etching that template metal. By repeating such a sequential process of overgrowth followed by etching, nanomatryoshka with multiple shells is produced. Notably, the spacing between the shells is determined by the thickness of the grown template. In general, the LSPR peaks of nano-matryoshka red shift as the spacing between shells or number of shells increases. For instance, in a work by Haddadnezhad et al.,<sup>60</sup> Au double-walled nanoframes containing wall frames nested inside one another in a core-shell manner were prepared. This structure was achieved by first synthesis of a Pt double-walled frame of truncated octahedron shape (Figure 4a), followed by regrowth of Au using the as-formed Pt frame as a seed. By controlling the amount of Au grown on the Pt seed, the gap distance between the inner and outer frames of an individual Au double-walled nanoframe can be adjusted in the range of 5.2-9.7 nm (Figure 4b-d). As the gap distance was increased, the major LSPR peak red shifted (Figure 4e).

To obtain PHNs with integrated inner shells, one effective method is the above-mentioned template regeneration approach (Figure 1c), where an inner shell is formed by selectively depositing metal atoms on the inner surfaces of a preformed hollow nanostructure as the seed. By adjusting the thickness of inner shell, the LSPR peaks of final products can be efficiently turned. Notably, during the course of LSPR tuning, the outer diameter and external shape of the hollow nanostructures remain unchanged. In a recent work by our group, \(^1\times48 \text{ nm Ag@Ag-Au shell@shell nanocages were synthesized through selective deposition of Ag atoms onto the inner surfaces of preformed Ag-Au nanocages (Figure 4f). The thickness of the inner Ag shell can be conveniently tuned in the range of 0-10.0 nm by controlling the amount of Ag adatoms. As the thickness of inner Ag shell was increased, the color of the Ag@Ag-Au nanocage suspensions also changed dramatically. A distinct color change from cyan to blue, violet, magenta, red, orange, and yellow could be distinguished by the naked eye (Figure 4g). As shown by Figure 4h, the major LSPR peaks of corresponding Ag@Ag-Au nanocage samples continuously blue shifted from ~695 nm to ~475 nm.

## 4. APPLICATIONS

PHNs with carefully engineered internal structures have been extensively used in various

technologically important applications. In this section, we highlight their applications in biosensing and photocatalysis, where the emphasis is placed on structure-performance relationship. Since GRR-based synthetic methods are more versatile than those non-GRR based methods in terms of controlling the internal structure of PHNs, in the following we primarily focus on examples of PHNs that are prepared by GRR-based methods.

#### 4.1. Application in Biosensing

In biosensing applications, plasmonic nanostructures are often used as labels or signal transducers, which provide optical signals to reflect the amount of biomarkers in a sample. In many biosensing platforms, PHNs offer superior performance relative to their solid counterparts owing to their superior plasmonic properties.

One of the commonly used biosensing technologies is lateral flow assay (LFA, Figure 5a), which offers rapid tests at low costs. 106,123-126 In most commercial LFAs, spherical Au nanoparticles (Au NPs, which typically have a diameter of ~40 nm and a major LSPR peak at ~530 nm) are used as labels. 127-130 However, the detection sensitivity of conventional Au NP-based LFA is relatively low, primarily due to the limited plasmonic activity of Au NPs. In a recent study, Ag-Au nanocages were developed and used as alternative labels to improve the sensitivity of LFA.<sup>2</sup> Those Ag-Au nanocages had a thick wall of 17.6 nm that consisted of five consecutive Ag-Au alloyed layers (Figure 5b). As shown by Figure 5c, the nanocages had a major LSPR peak located at ~551 nm and displayed a red color, similar to those of 40 nm Au NPs. Significantly, the LSPR extinction of these nanocages was found to be 10 times larger than that of 40 nm Au NPs, resulting in a much more intense red color for these nanocages compared to Au NPs. Using human prostate-specific antigen (PSA) as a model biomarker, the nanocages-based LFA offered a low limit of detection (LOD) of 0.1 ng/mL (Figure 5d). In comparison, the LOD of conventional Au NP-based LFA was determined to be ~1.0 ng/mL. This considerable improvement in detection sensitivity can be ascribed to the superior plasmonic activity of the nanocages relative to Au NPs given that all other components of the two LFAs (e.g., antibodies and materials of test strip) were kept the same.

In another biosensing system (Figure 6a), Ag@Ag-Au shell@shell nanocages were used as colorimetric labels for the detection of human carcinoembryonic antigen (CEA, a cancer biomarker). Briefly, CEA in a sample is specifically captured by antibodies conjugated with alkaline phosphatase (ALP, an enzyme that can catalyze the formation of ascorbic acid). When incubated with solutions containing AgNO<sub>3</sub> (a precursor to Ag) and Ag-Au nanocages, the formed

ascorbic acid as a reducing agent could activate the selective growth of Ag towards the inner surfaces of the nanocages, resulting in the formation of Ag@Ag-Au shell@shell nanocages. The thickness of inner Ag shell is determined by the amount of ascorbic acid yielded in the reaction solution, which is correlated to the concentration of CEA in a sample. The Ag@Ag-Au nanocages of various Ag shell thicknesses displayed different colors that could be visualized by the naked eye (for semi-quantitative analysis) or quantified by a UV-vis spectrophotometer (for quantitative analysis). By referring to the blank of 0 ng/mL CEA (cyan color), the naked-eye LOD was about 2 ng/mL (Figure 6b). Quantitative analysis based on the shift of major LSPR peaks offered a lower LOD at 0.14 ng/mL (Figure 6c,d). This LOD was ~3-fold lower than the LOD of conventional ALP-based enzyme-linked immunosorbent assay (ELISA) that used the same antibodies and similar assay procedures. The outstanding performance of this biosensing system relies on the sensitive LSPR peak shift as a response to the change of the thickness of inner Ag shell. When the same amount of Ag was grown on solid nanoparticles such as Au nanospheres and nanorods, the shift of LSPR peaks was not as sensitive as in the case of growing Ag inside a nanocage (Figure 6e). These experimental observations were consistent with calculation results based on finitedifference time-domain (FDTD) simulations.

## 4.2. Application in Photocatalysis

With the increase of energy demand and environmental pollution, the harvesting of clean and sustainable solar energy has been extensively studied over the years. <sup>131</sup> Photocatalysis is designed to produce solar fuels such as hydrogen through a water-splitting process, where PHNs are promising candidates due to their unique plasmonic and structural properties.

PHNs are usually coupled with semiconductor particles or layers on the surface when used as photocatalysts. There are many benefits from the coupling of PHNs and semiconductors. For instance, the introduction of PHNs can extend the absorption spectrum of the photocatalysts to broader visible region of solar light. Plasmonic metals can trigger the generation of additional electron-hole pairs in the semiconductor interface through a plasma-induced resonance energy transfer (PRET) mechanism, hus improving the photocatalytic efficiency. Moreover, the hollow structures of PHNs endow photocatalysts with unique and useful characteristics: the hollow interiors produce light scattering and hence facilitate light harvesting; The thin shells of PHNs reduce the transport distance of charge carriers, thereby minimizing the energy loss by reducing

the charge recombination during transportation; PHNs possess high specific surface areas which increase the number of active sites and thus catalytic performance; The shells of PHNs separate the external space and the internal voids so that the two half-reactions are spatially separated.<sup>31,134</sup>

Most abovementioned benefits of photocatalysts made of PHN-semiconductor composites have a strong dependence on the internal structures of PHNs. As such, engineering the internal structure of a PHN represents a powerful approach to optimize the efficiency of photocatalysis. For example, in a recent work by Yue et al., <sup>69</sup> Au-Ag hollow nanoparticles (HNPs) with different internal void sizes in the range of 35-20 nm (Figure 7a) were synthesized through a synthetic strategy based on GRR and co-reduction. Photocatalysts for H<sub>2</sub> evolution were prepared by coupling the Au-Ag HNPs with titanium oxide (TiO<sub>2</sub>, P25). As shown by Figure 7b, major LSPR peaks of the Au-Ag HNPs blue shifted from 713 nm to 490 nm as the void size decreased from 35 to 20 nm. The photocatalysis results (Figure 7c) showed that all the Au-Ag HNP/P25 composites displayed higher photocatalytic activities under full spectrum illumination than pure P25. The improvement of photocatalytic performance by Au-Ag HNPs was believed to arise from the hot spots generated by electromagnetic fields. Notably, a maximal photocatalytic activity was observed with an Au-Ag HNP that had a moderate void size (sample ii in Figure 7a). This is mainly because this HNP has a complete shell and can yield a stronger electromagnetic field to promote charge separation. As the void of HNP increased (e.g., sample i in Figure 7a), pores in the shell present, which reduced the electromagnetic field strength and thus the photocatalytic activity. As the void of HNP decreased (e.g., samples iii and iv in Figure 7a), the interaction between the sphere and cavity plasmon weakened and this further weakened the electromagnetic field. This study clearly demonstrates the photocatalytic activity of PHNs is closely related to their internal structure.

## 5. CONCLUSIONS

In this perspective, we provide a comprehensive discussion on engineering the internal structure of plasmonic hollow nanostructures (PHNs) for enhanced plasmonic properties. Most of the PHNs were synthesized *via* the galvanic replacement reaction (GRR)-based methods. To construct highly diverse internal structures of the PHNs, GRRs are often combined with other mechanisms such as co-reduction, template regeneration, Kirkendall effect, and regulation of reduction potential. There are several key parameters of internal structure that are directly correlated to the plasmonic properties of PHNs, including the morphology of internal void,

elemental composition of walls, wall thickness, and inner shell structure. Precise control over these parameters yields PHNs with superior extinction intensities and a wide LSPR peak tuning range, facilitating their applications in various applications such as biosensing and photocatalysis.

Despite the current progress in engineering the internal structures of PHNs, there are still challenges and opportunities in this field. Examples include: i) Controlling the crystallinity of walls of PHNs. Crystallinity of PHNs may influence their performance in certain applications, especially in catalysis. 135,136 Currently, due to the self-templating nature of galvanic replacement reactions, the crystallinity of resultant PHNs cannot be fully controlled. Especially, when the two metals involved in a GRR have a large lattice mismatch, the hollow nanostructures as products tend to have a polycrystalline structure with randomly distributed defects in the walls.<sup>39</sup> It is meaningful to explore effective approaches for controlling the crystallinity of PHNs in the future; ii) Improving the uniformity of PHNs. Good uniformity, in terms of morphology, structure, and elemental composition, is critical to ensure reliable and consistent performance of PHNs in certain applications. In particular, it is challenging to achieve uniform internal structures for PHNs produced in different batches of synthesis. This is primarily because controlling the internal structure requires careful manipulations of various thermodynamic and kinetic parameters during a synthesis. A slight variation in experimental conditions can lead to significantly different internal structures; iii) Enhancing the stability of PHNs. In some applications (e.g., those rely on laser irradiations), PHNs experience extremely high temperatures and may subject to morphological changes. To maintain their structures and plasmonic properties, it is vital to enhance the thermal stability of PHNs. Incorporating a thermally stable metal (e.g., Pt, Ru, Rh, and Ir) into PHNs may enhance the stability. 137-141 Moreover, PHNs may tend to aggregate when stored in solution phase for a long period of time. It is of significance to select appropriate colloidal stabilizers to improve the long-term stability; iv) Scaling up the synthesis. Currently, most syntheses of PHNs with complex structures remain at the laboratory scale, wherein each step is carefully and precisely controlled. Scaling up the synthesis without compromising the quality and uniformity of PHNs is necessary for industrial applications. Recent efforts on continuous flow synthesis based on droplets may open a new avenue for scaling up the production of PHNs. 142-145 We hope this paper will inspire new basic and applied research in the field of plasmonic nanostructures in the future.

#### **Notes**

The authors declare no competing financial interests.

#### **ACKNOWLEDGMENTS**

This work was supported in part by the grants from the National Science Foundation (NSF) (DMR-2004546 and CBET-2234873) and startup funds from the University of Central Florida (UCF).

## **Author Biographies**

**Dr. Xiaohu Xia** is currently an Associate Professor in the chemistry department at University of Central Florida (UCF). He holds a joint appointment in the NanoScience Technology Center at UCF. Prior to his appointment at UCF, he worked at Michigan Technological University as an Assistant Professor during 2014-2018. He received his Ph.D. in Biochemistry and Molecular Biology from Xiamen University, China in 2011. He worked at Georgia Tech as a Postdoctoral Fellow from 2012 to 2014. His current research interests include materials chemistry, nanoscience/technology, and medical diagnostics. He has co-authored more than 70 peer-reviewed journal articles that have been cited more than 10,000 times.

**Dr. Shikuan Shao** is currently a postdoctoral fellow at the University of Central Florida (UCF), working with Prof. Xiaohu Xia. He received his Ph.D. in Chemistry from UCF in 2024. He received his MS in Chemical Engineering from State University of New York - University at Buffalo in 2018. His research interests include the design and synthesis of functionalized nanomaterials for biosensing and catalytic applications.

#### REFERENCES

1. Gao, Z.; Shao, S.; Gao, W.; Tang, D.; Tang, D.; Zou, S.; Kim, M. J.; Xia, X. Morphology-Invariant Metallic Nanoparticles with Tunable Plasmonic Properties. *ACS Nano* **2021**, *15*, 2428-2438.

- 2. Gao, Z.; Ye, H.; Wang, Q.; Kim, M. J.; Tang, D.; Xi, Z.; Wei, Z.; Shao, S.; Xia, X. Template Regeneration in Galvanic Replacement: A Route to Highly Diverse Hollow Nanostructures. *ACS Nano* **2020**, *14*, 791-801.
- 3. Chen, J.; Glaus, C.; Laforest, R.; Zhang, Q.; Yang, M.; Gidding, M.; Welch, M. J.; Xia, Y. Gold Nanocages as Photothermal Transducers for Cancer Treatment. *Small* **2010**, *6*, 811-817.
- 4. Skrabalak, S. E.; Chen, J.; Au, L.; Lu, X.; Li, X.; Xia, Y. Gold Nanocages for Biomedical Applications. *Adv. Mater.* **2007**, *19*, 3177-3184.
- 5. Xia, X.; Xia, Y. Gold Nanocages as Multifunctional Materials for Nanomedicine. *Front. Phys.* **2013**, *9*, 378-384.
- Yavuz, M. S.; Cheng, Y.; Chen, J.; Cobley, C. M.; Zhang, Q.; Rycenga, M.; Xie, J.; Kim, C.;
  Song, K. H.; Schwartz, A. G.; et al. Gold Nanocages Covered by Smart Polymers for
  Controlled Release with Near-Infrared Light. *Nat. Mater.* 2009, 8, 935-939.
- 7. Zhu, D.; Liu, Y.; Liu, M.; Liu, X.; Prasad, P. N.; Swihart, M. T. Galvanic Replacement Synthesis of Multi-Branched Gold Nanocrystals for Photothermal Cancer Therapy. *J. Mater. Chem. B* **2020**, *8*, 5491-5499.
- 8. Wang, C.; Wang, Y.; Zhang, L.; Miron, R. J.; Liang, J.; Shi, M.; Mo, W.; Zheng, S.; Zhao, Y.; Zhang, Y. Pretreated Macrophage-Membrane-Coated Gold Nanocages for Precise Drug Delivery for Treatment of Bacterial Infections. *Adv. Mater.* **2018**, *30*, e1804023.
- 9. Abadeer, N. S.; Murphy, C. J. Recent Progress in Cancer Thermal Therapy Using Gold Nanoparticles. *J. Phys. Chem. C* **2016**, *120*, 4691-4716.
- 10. Ai, K.; Huang, J.; Xiao, Z.; Yang, Y.; Bai, Y.; Peng, J. Localized Surface Plasmon Resonance Properties and Biomedical Applications of Copper Selenide Nanomaterials. *Mater. Today Chem.* **2021**, *20*, 100402.
- 11. Li, C.; Jin, Y. Shell-Isolated Plasmonic Nanostructures for Biosensing, Catalysis, and Advanced Nanoelectronics. *Adv. Funct. Mater.* **2021**, *31*, 2008031.
- 12. Hu, F.; Zhang, Y.; Chen, G.; Li, C.; Wang, Q. Double-Walled Au Nanocage/SiO<sub>2</sub> Nanorattles: Integrating SERS Imaging, Drug Delivery and Photothermal Therapy. *Small* **2015**, *11*, 985-993.
- 13. Lal, S.; Grady, N. K.; Kundu, J.; Levin, C. S.; Lassiter, J. B.; Halas, N. J. Tailoring Plasmonic Substrates for Surface Enhanced Spectroscopies. *Chem. Soc. Rev.* **2008**, *37*, 898-911.
- 14. da Silva, A. G. M.; Rodrigues, T. S.; Haigh, S. J.; Camargo, P. H. C. Galvanic Replacement

- Reaction: Recent Developments for Engineering Metal Nanostructures towards Catalytic Applications. *Chem. Commun.* **2017**, *53*, 7135-7148.
- 15. Wang, J.; Cui, Y.; Wang, D. Design of Hollow Nanostructures for Energy Storage, Conversion and Production. *Adv. Mater.* **2019**, *31*, e1801993.
- 16. Prodan, E.; Nordlander, P. Plasmon Hybridization in Spherical Nanoparticles. *J. Chem. Phys.* **2004**, *120*, 5444-5454.
- 17. Prodan, E.; Nordlander, P. Structural Tunability of the Plasmon Resonances in Metallic Nanoshells. *Nano Lett.* **2003**, *3*, 543-547.
- 18. Prodan, E.; Nordlander, P.; Halas, N. J. Electronic Structure and Optical Properties of Gold Nanoshells. *Nano Lett.* **2003**, *3*, 1411-1415.
- 19. Prodan, E.; Radloff, C.; Halas, N. J.; Nordlander, P. A Hybridization Model for the Plasmon Response of Complex Nanostructures. *Science* **2003**, *302*, 419-422.
- 20. Halas, N. J.; Lal, S.; Chang, W.-S.; Link, S.; Nordlander, P. Plasmons in Strongly Coupled Metallic Nanostructures. *Chem. Rev.* **2011**, *111*, 3913-3961.
- 21. Rycenga, M.; Cobley, C. M.; Zeng, J.; Li, W.; Moran, C. H.; Zhang, Q.; Qin, D.; Xia, Y. Controlling the Synthesis and Assembly of Silver Nanostructures for Plasmonic Applications. *Chem. Rev.* **2011**, *111*, 3669-3712.
- 22. Mayer, K. M.; Hafner, J. H. Localized Surface Plasmon Resonance Sensors. *Chem. Rev.* **2011**, *111*, 3828-3857.
- 23. Kelly, K. L.; Coronado, E.; Zhao, L. L.; Schatz, G. C. The Optical Properties of Metal Nanoparticles: The Influence of Size, Shape, and Dielectric Environment. *J. Phys. Chem. B* **2003**, *107*, 668-677.
- 24. Halas, N. Playing with Plasmons: Tuning the Optical Resonant Properties of Metallic Nanoshells. *MRS Bull.* **2005**, *30*, 362-367.
- 25. Xia, X.; Wang, Y.; Ruditskiy, A.; Xia, Y. 25th Anniversary Article: Galvanic Replacement: A Simple and Versatile Route to Hollow Nanostructures with Tunable and Well-Controlled Properties. *Adv. Mater.* **2013**, *25*, 6313-6333.
- Genç, A.; Patarroyo, J.; Sancho-Parramon, J.; Bastús, N. G.; Puntes, V.; Arbiol, J. Hollow Metal Nanostructures for Enhanced Plasmonics: Synthesis, Local Plasmonic Properties and Applications. *Nanophotonics* 2017, 6, 193-213.
- 27. Cobley, C. M.; Campbell, D. J.; Xia, Y. Tailoring the Optical and Catalytic Properties of

- Gold-Silver Nanoboxes and Nanocages by Introducing Palladium. *Adv. Mater.* **2008**, *20*, 748-752.
- 28. Park, J. M.; Choi, H. E.; Kudaibergen, D.; Kim, J. H.; Kim, K. S. Recent Advances in Hollow Gold Nanostructures for Biomedical Applications. *Front. Chem.* **2021**, *9*, 699284.
- 29. Xiao, M.; Wang, Z.; Lyu, M.; Luo, B.; Wang, S.; Liu, G.; Cheng, H. M.; Wang, L. Hollow Nanostructures for Photocatalysis: Advantages and Challenges. *Adv. Mater.* **2019**, *31*, e1801369.
- 30. Cobley, C. M.; Xia, Y. Engineering the Properties of Metal Nanostructures *via* Galvanic Replacement Reactions. *Mater. Sci. Eng. R Rep.* **2010**, 70, 44-62.
- 31. Wang, X.; Feng, J.; Bai, Y.; Zhang, Q.; Yin, Y. Synthesis, Properties, and Applications of Hollow Micro-/Nanostructures. *Chem. Rev.* **2016**, *116*, 10983-11060.
- 32. Ruan, Q.; Shao, L.; Shu, Y.; Wang, J.; Wu, H. Growth of Monodisperse Gold Nanospheres with Diameters from 20 nm to 220 nm and Their Core/Satellite Nanostructures. *Adv. Opt. Mater.* **2013**, *2*, 65-73.
- 33. Zhang, Q.; Li, W.; Moran, C.; Zeng, J.; Chen, J.; Wen, L.-P.; Xia, Y. Seed-Mediated Synthesis of Ag Nanocubes with Controllable Edge Lengths in the Range of 30-200 nm and Comparison of Their Optical Properties. *J. Am. Chem. Soc.* **2010**, *132*, 11372-11378.
- 34. Orendorff, C. J.; Sau, T. K.; Murphy, C. J. Shape-Dependent Plasmon-Resonant Gold Nanoparticles. *Small* **2006**, *2*, 636-639.
- 35. Qin, F.; Zhao, T.; Jiang, R.; Jiang, N.; Ruan, Q.; Wang, J.; Sun, L. D.; Yan, C. H.; Lin, H. Q. Thickness Control Produces Gold Nanoplates with Their Plasmon in the Visible and Near-Infrared Regions. *Adv. Opt. Mater.* **2015**, *4*, 76-85.
- 36. Rodríguez-Lorenzo, L.; Romo-Herrera, J. M.; Pérez-Juste, J.; Alvarez-Puebla, R. A.; Liz-Marzán, L. M. Reshaping and LSPR Tuning of Au Nanostars in the Presence of CTAB. *J. Mater. Chem.* **2011**, *21*, 11544-11549.
- 37. Rodriguez-Lorenzo, L.; de la Rica, R.; Alvarez-Puebla, R. A.; Liz-Marzan, L. M.; Stevens, M. M. Plasmonic Nanosensors with Inverse Sensitivity by Means of Enzyme-Guided Crystal Growth. Nat. Mater. **2012**, *11*, 604-607.
- 38. Sutter, E.; Jungjohann, K.; Bliznakov, S.; Courty, A.; Maisonhaute, E.; Tenney, S.; Sutter, P. *In Situ* Liquid-Cell Electron Microscopy of Silver-Palladium Galvanic Replacement Reactions on Silver Nanoparticles. *Nat. Commun.* **2014**, *5*, 4946.

- 39. Cheng, H.; Wang, C.; Qin, D.; Xia, Y. Galvanic Replacement Synthesis of Metal Nanostructures: Bridging the Gap between Chemical and Electrochemical Approaches. *Acc. Chem. Res.* **2023**, *56*, 900-909.
- 40. Goris, B.; Polavarapu, L.; Bals, S.; Van Tendeloo, G.; Liz-Marzan, L. M. Monitoring Galvanic Replacement through Three-Dimensional Morphological and Chemical Mapping. *Nano Lett.* **2014**, *14*, 3220-3226.
- 41. Oh, M. H.; Yu, T.; Yu, S.-H.; Lim, B.; Ko, K.-T.; Willinger, M.-G.; Seo, D.-H.; Kim, B. H.; Cho, M. G.; Park, J.-H.; et al. Galvanic Replacement Reactions in Metal Oxide Nanocrystals. *Science* **2013**, *340*, 964-968.
- 42. Gonzalez, E.; Arbiol, J.; Puntes, V. F. Carving at the Nanoscale: Sequential Galvanic Exchange and Kirkendall Growth at Room Temperature. *Science* **2011**, *334*, 1377-1380.
- 43. Lee, S.; Sim, K.; Moon, S. Y.; Choi, J.; Jeon, Y.; Nam, J. M.; Park, S. J. Controlled Assembly of Plasmonic Nanoparticles: From Static to Dynamic Nanostructures. *Adv. Mater.* **2021**, *33*, e2007668.
- 44. Ouyang, R.; Liu, J. X.; Li, W. X. Atomistic Theory of Ostwald Ripening and Disintegration of Supported Metal Particles under Reaction Conditions. *J. Am. Chem. Soc.* **2013**, *135*, 1760-1771.
- 45. Yec, C. C.; Zeng, H. C. Synthesis of Complex Nanomaterials *via* Ostwald Ripening. *J. Mater. Chem. A* **2014**, *2*, 4843-4851.
- Yu, L.; Han, R.; Sang, X.; Liu, J.; Thomas, M. P.; Hudak, B. M.; Patel, A.; Page, K.; Guiton,
  B. S. Shell-Induced Ostwald Ripening: Simultaneous Structure, Composition, and
  Morphology Transformations during the Creation of Hollow Iron Oxide Nanocapsules. ACS
  Nano 2018, 12, 9051-9059.
- 47. Wang, Z.; Yu, R. Hollow Micro/Nanostructured Ceria-Based Materials: Synthetic Strategies and Versatile Applications. *Adv. Mater.* **2019**, *31*, 1800592.
- 48. Schmidt, O. G.; Eberl, K. Thin Solid Films Roll Up into Nanotubes. *Nature* **2001**, *410*, 168-168.
- 49. Barclay, T. G.; Constantopoulos, K.; Matisons, J. Nanotubes Self-Assembled from Amphiphilic Molecules *via* Helical Intermediates. *Chem. Rev.* **2014**, *114*, 10217-10291.
- 50. Aherne, D.; Gara, M.; Kelly, J. M.; Gun'ko, Y. K. From Ag Nanoprisms to Triangular AuAg Nanoboxes. *Adv. Funct. Mater.* **2010**, *20*, 1329-1338.

- 51. Moreau, L. M.; Schurman, C. A.; Kewalramani, S.; Shahjamali, M. M.; Mirkin, C. A.; Bedzyk, M. J. How Ag Nanospheres Are Transformed into AgAu Nanocages. *J. Am. Chem. Soc.* **2017**, *139*, 12291-12298.
- 52. Xia, Y.; Li, W.; Cobley, C. M.; Chen, J.; Xia, X.; Zhang, Q.; Yang, M.; Cho, E. C.; Brown, P. K. Gold Nanocages: From Synthesis to Theranostic Applications. *Acc. Chem. Res.* **2011**, 44, 914-924.
- 53. Skrabalak, S. E.; Au, L.; Li, X.; Xia, Y. Facile Synthesis of Ag Nanocubes and Au Nanocages. *Nat. Protoc.* **2007**, *2*, 2182-2190.
- 54. Huang, L.; Wan, J.; Wei, X.; Liu, Y.; Huang, J.; Sun, X.; Zhang, R.; Gurav, D. D.; Vedarethinam, V.; Li, Y.; et al. Plasmonic Silver Nanoshells for Drug and Metabolite Detection. *Nat. Commun.* **2017**, *8*, 220.
- 55. Russo, L.; Merkoçi, F.; Patarroyo, J.; Piella, J.; Merkoçi, A.; Bastús, N. G.; Puntes, V. Time-and Size-Resolved Plasmonic Evolution with nm Resolution of Galvanic Replacement Reaction in AuAg Nanoshells Synthesis. *Chem. Mater.* **2018**, *30*, 5098-5107.
- 56. Ye, H.; Nowak, C.; Liu, Y.; Li, Y.; Zhang, T.; Bleris, L.; Qin, Z. Plasmonic LAMP: Improving the Detection Specificity and Sensitivity for SARS-CoV-2 by Plasmonic Sensing of Isothermally Amplified Nucleic Acids. *Small* **2022**, *18*, e2107832.
- 57. Garcia-Leis, A.; Torreggiani, A.; Garcia-Ramos, J. V.; Sanchez-Cortes, S. Hollow Au/Ag Nanostars Displaying Broad Plasmonic Resonance and High Surface-Enhanced Raman Sensitivity. *Nanoscale* **2015**, *7*, 13629-13637.
- 58. Ngo, N. M.; Omidiyan, M.; Tran, H.-V.; Lee, T. R. Stable Semi-Hollow Gold-Silver Nanostars with Tunable Plasmonic Resonances Ranging from Ultraviolet-Visible to Near-Infrared Wavelengths: Implications for Photocatalysis, Biosensing, and Theranostics. *ACS Appl. Nano Mater.* **2022**, *5*, 11391-11399.
- 59. Au, L.; Chen, Y.; Zhou, F.; Camargo, P. H.; Lim, B.; Li, Z. Y.; Ginger, D. S.; Xia, Y. Synthesis and Optical Properties of Cubic Gold Nanoframes. *Nano Res.* **2008**, *1*, 441-449.
- 60. Haddadnezhad, M.; Jung, I.; Park, W.; Lee, J. W.; Park, W.; Kim, J.; Park, S. Plasmonic Double-Walled Nanoframes with Face-to-Face Nanogaps for Strong SERS Activity. *Nano Lett.* **2023**, *23*, 6831-6838.
- 61. Shi, Q.; Fu, R.; Sikdar, D.; Perera, T.; Chesman, A. S. R.; Yong, Z.; Lu, Y.; Liu, Y.; Guo, Z.; Gong, S.; et al. Two-Dimensional Nanoassemblies from Plasmonic Matryoshka Nanoframes.

- J. Phys. Chem. C 2021, 125, 27753-27762.
- 62. Xu, J.; Xu, H.; Xu, L.; Ruan, Q.; Zhu, X.; Kan, C.; Shi, D. Plasmonic and Catalytic Au NBP@AgPd Nanoframes for Highly Efficient Photocatalytic Reactions. *Phys. Chem. Chem. Phys.* **2023**, *25*, 13189-13197.
- 63. Go, S.; Yoo, S.; Son, J.; Lee, S.; Lee, J.; Lee, S.; Kim, J.; Park, M.; Park, W.; Kim, J. M.; et al. Ring-in-a-Triangle Nanoframes: Integrating with Intra- and Interhotspots for Highly Amplified Near-Field Focusing. *Nano Lett.* **2022**, *22*, 1734-1740.
- 64. Ham, S.; Jang, H. J.; Song, Y.; Shuford, K. L.; Park, S. Octahedral and Cubic Gold Nanoframes with Platinum Framework. *Angew. Chem.* **2015**, *54*, 9025-9028.
- 65. Dreaden, E. C.; Alkilany, A. M.; Huang, X.; Murphy, C. J.; El-Sayed, M. A. The Golden Age: Gold Nanoparticles for Biomedicine. *Chem. Soc. Rev.* **2012**, *41*, 2740-2779.
- 66. Wu, H.; Bu, T.; Sun, B.; Xi, J.; Cao, Y.; Wang, Y.; Xuan, C.; Feng, Q.; Yan, H.; Wang, L. "Three-in-One" Multifunctional Hollow Nanocages with Colorimetric Photothermal Catalytic Activity for Enhancing Sensitivity in Biosensing. *Anal. Chem.* **2024**, *96*, 4825-4834.
- 67. Prieto, G.; Tuysuz, H.; Duyckaerts, N.; Knossalla, J.; Wang, G. H.; Schuth, F. Hollow Nanoand Microstructures as Catalysts. *Chem. Rev.* **2016**, *116*, 14056-14119.
- 68. Amirjani, A.; Amlashi, N. B.; Ahmadiani, Z. S. Plasmon-Enhanced Photocatalysis Based on Plasmonic Nanoparticles for Energy and Environmental Solutions: A Review. *ACS Appl. Nano Mater.* **2023**, *6*, 9085-9123.
- 69. Yue, X.; Hou, J.; Zhao, H.; Wu, P.; Guo, Y.; Shi, Q.; Chen, L.; Peng, S.; Liu, Z.; Cao, G. Au-Ag Alloy Nanoparticles with Tunable Cavity for Plasmon-Enhanced Photocatalytic H<sub>2</sub> Evolution. *J. Energy Chem.* **2020**, *49*, 1-7.
- 70. Zhu, Z.; Luo, H.; Wang, T.; Zhang, C.; Liang, M.; Yang, D.; Liu, M.; Yu, W. W.; Bai, Q.; Wang, L.; et al. Plasmon-Enhanced Peroxidase-like Activity of Nitrogen-Doped Graphdiyne Oxide Quantum Dots/Gold-Silver Nanocage Heterostructures for Antimicrobial Applications. *Chem. Mater.* **2022**, *34*, 1356-1368.
- 71. Yue, X.; Hou, J.; Zhang, Y.; Wu, P.; Guo, Y.; Peng, S.; Liu, Z.; Jiang, H. Improved CdS Photocatalytic H<sub>2</sub> Evolution Using Au-Ag Nanoparticles with Tunable Plasmon-Enhanced Resonance Energy Transfer. *Dalton Trans.* **2020**, *49*, 7467-7473.
- 72. Zhao, X.; Wang, S.; Yang, K.; Yang, X.; Liu, X. Controlled Gold-Palladium Cores in Ceria Hollow Spheres as Nanoreactor for Plasmon-Enhanced Catalysis under Visible Light

- Irradiation. J. Colloid Interface Sci. 2023, 633, 11-23.
- 73. Mo, W.; Fan, Z.; Zhong, S.; Chen, W.; Hu, L.; Zhou, H.; Zhao, W.; Lin, H.; Ge, J.; Chen, J.; et al. Embedding Plasmonic Metal into Heterointerface of MOFs-Encapsulated Semiconductor Hollow Architecture for Boosting CO<sub>2</sub> Photoreduction. *Small* **2023**, *19*, e2207705.
- 74. Feng, J.; Yin, Y. Self-Templating Approaches to Hollow Nanostructures. *Adv. Mater.* **2019**, *31*, 1802349.
- 75. Polavarapu, L.; Zanaga, D.; Altantzis, T.; Rodal-Cedeira, S.; Pastoriza-Santos, I.; Perez-Juste, J.; Bals, S.; Liz-Marzan, L. M. Galvanic Replacement Coupled to Seeded Growth as a Route for Shape-Controlled Synthesis of Plasmonic Nanorattles. *J. Am. Chem. Soc.* 2016, 138, 11453-11456.
- 76. Park, J. E.; Kim, S.; Son, J.; Lee, Y.; Nam, J. M. Highly Controlled Synthesis and Super-Radiant Photoluminescence of Plasmonic Cube-in-Cube Nanoparticles. *Nano Lett.* **2016**, *16*, 7962-7967.
- 77. J, R. D.; McCarthy, L. A.; Ringe, E.; Boudreau, D. Enhanced Control of Plasmonic Properties of Silver-Gold Hollow Nanoparticles *via* a Reduction-Assisted Galvanic Replacement Approach. *RSC Adv.* **2018**, *9*, 389-396.
- 78. Xia, Y.; Xia, X.; Peng, H. C. Shape-Controlled Synthesis of Colloidal Metal Nanocrystals: Thermodynamic *versus* Kinetic Products. *J. Am. Chem. Soc.* **2015**, *137*, 7947-7966.
- 79. Xia, X.; Xie, S.; Liu, M.; Peng, H. C.; Lu, N.; Wang, J.; Kim, M. J.; Xia, Y. On the Role of Surface Diffusion in Determining the Shape or Morphology of Noble-Metal Nanocrystals. *Proc. Natl. Acad. Sci. U.S.A.* **2013**, *110*, 6669-6673.
- 80. Ye, H.; Wang, Q.; Catalano, M.; Lu, N.; Vermeylen, J.; Kim, M. J.; Liu, Y.; Sun, Y.; Xia, X. Ru Nanoframes with an fcc Structure and Enhanced Catalytic Properties. *Nano Lett.* **2016**, *16*, 2812-2817.
- 81. Jing, H.; Wang, H. Structural Evolution of Ag-Pd Bimetallic Nanoparticles through Controlled Galvanic Replacement: Effects of Mild Reducing Agents. *Chem. Mater.* **2015**, *27*, 2172-2180.
- 82. Yadav, V.; Jeong, S.; Ye, X.; Li, C. W. Surface-Limited Galvanic Replacement Reactions of Pd, Pt, and Au onto Ag Core Nanoparticles through Redox Potential Tuning. *Chem. Mater.* **2022**, *34*, 1897-1904.

- 83. Matsusaki, M.; Ajiro, H.; Kida, T.; Serizawa, T.; Akashi, M. Layer-by-Layer Assembly Through Weak Interactions and Their Biomedical Applications. *Adv. Mater.* **2012**, *24*, 454-474.
- 84. He, J.; Huang, X.; Li, Y.-C.; Liu, Y.; Babu, T.; Aronova, M. A.; Wang, S.; Lu, Z.; Chen, X.; Nie, Z. Self-Assembly of Amphiphilic Plasmonic Micelle-Like Nanoparticles in Selective Solvents. *J. Am. Chem. Soc.* **2013**, *135*, 7974-7984.
- 85. Wei, J.; Niikura, K.; Higuchi, T.; Kimura, T.; Mitomo, H.; Jinnai, H.; Joti, Y.; Bessho, Y.; Nishino, Y.; Matsuo, Y.; et al. Yolk/Shell Assembly of Gold Nanoparticles by Size Segregation in Solution. *J. Am. Chem. Soc.* **2016**, *138*, 3274-3277.
- 86. Niikura, K.; Iyo, N.; Higuchi, T.; Nishio, T.; Jinnai, H.; Fujitani, N.; Ijiro, K. Gold Nanoparticles Coated with Semi-Fluorinated Oligo(ethylene glycol) Produce sub-100 nm Nanoparticle Vesicles without Templates. *J. Am. Chem. Soc.* **2012**, *134*, 7632-7635.
- 87. Hickey, R. J.; Seo, M.; Luo, Q.; Park, S. J. Directional Self-Assembly of Ligand-Stabilized Gold Nanoparticles into Hollow Vesicles through Dynamic Ligand Rearrangement. *Langmuir* **2015**, *31*, 4299-4304.
- 88. Manna, U.; Lee, J. H.; Deng, T. S.; Parker, J.; Shepherd, N.; Weizmann, Y.; Scherer, N. F. Selective Induction of Optical Magnetism. *Nano Lett.* **2017**, *17*, 7196-7206.
- 89. Li, C.; Lee, S.; Qian, Z.; Woods, C.; Park, S.-J.; Fakhraai, Z. Controlling Magnetic Dipole Resonance in Raspberry-like Metamolecules. *J. Phys. Chem. C* **2018**, *122*, 6808-6817.
- 90. Lee, S.; Woods, C. N.; Ibrahim, O.; Kim, S. W.; Pyun, S. B.; Cho, E. C.; Fakhraai, Z.; Park, S.-J. Distinct Optical Magnetism in Gold and Silver Probed by Dynamic Metamolecules. *J. Phys. Chem. C* **2020**, *124*, 20436-20444.
- 91. Mahmoud, M. A.; El-Sayed, M. A. Substrate Effect on the Plasmonic Sensing Ability of Hollow Nanoparticles of Different Shapes. *J Phys. Chem. B* **2013**, *117*, 4468-4477.
- 92. Jiang, Y.; Upputuri, P. K.; Xie, C.; Lyu, Y.; Zhang, L.; Xiong, Q.; Pramanik, M.; Pu, K. Broadband Absorbing Semiconducting Polymer Nanoparticles for Photoacoustic Imaging in Second Near-Infrared Window. *Nano Lett.* **2017**, *17*, 4964-4969.
- 93. Sun, T.; Dou, J.-H.; Liu, S.; Wang, X.; Zheng, X.; Wang, Y.; Pei, J.; Xie, Z. Second Near-Infrared Conjugated Polymer Nanoparticles for Photoacoustic Imaging and Photothermal Therapy. *ACS Appl. Mater. Interfaces* **2018**, *10*, 7919-7926.
- 94. Ding, X.; Liow, C. H.; Zhang, M.; Huang, R.; Li, C.; Shen, H.; Liu, M.; Zou, Y.; Gao, N.;

- Zhang, Z.; et al. Surface Plasmon Resonance Enhanced Light Absorption and Photothermal Therapy in the Second Near-Infrared Window. *J. Am. Chem. Soc.* **2014**, *136*, 15684-15693.
- 95. Smith, A. M.; Mancini, M. C.; Nie, S. Second Window for *In Vivo* Imaging. *Nat. Nanotechnol.* **2009**, *4*, 710-711.
- 96. Tsai, M.-F.; Chang, S.-H. G.; Cheng, F.-Y.; Shanmugam, V.; Cheng, Y.-S.; Su, C.-H.; Yeh, C.-S. Au Nanorod Design as Light-Absorber in the First and Second Biological Near-Infrared Windows for *In Vivo* Photothermal Therapy. *ACS Nano* **2013**, *7*, 5330-5342.
- 97. Cai, K.; Zhang, W.; Zhang, J.; Li, H.; Han, H.; Zhai, T. Design of Gold Hollow Nanorods with Controllable Aspect Ratio for Multimodal Imaging and Combined Chemo-Photothermal Therapy in the Second Near-Infrared Window. *ACS Appl. Mater. Interfaces* **2018**, *10*, 36703-36710.
- 98. Kim, S.; Kim, J. M.; Park, J. E.; Nam, J. M. Nonnoble-Metal-Based Plasmonic Nanomaterials: Recent Advances and Future Perspectives. *Adv. Mater.* **2018**, *30*, e1704528.
- 99. Qin, Z.; Zheng, Y.; Du, T.; Wang, Y.; Gao, H.; Quan, J.; Zhang, Y.; Du, Y.; Yin, L.; Wang, X.; et al. Cysteamine: A Key to Trigger Aggregation-Induced NIR-II Photothermal Effect and Silver Release Booming of Gold-Silver Nanocages for Synergetic Treatment of Multidrug-Resistant Bacteria Infection. *Chem. Eng. J.* **2021**, *414*, 128779.
- 100. Zhang, L.; Pan, J.; Long, Y.; Li, J.; Li, W.; Song, S.; Shi, Z.; Zhang, H. CeO<sub>2</sub>-Encapsulated Hollow Ag-Au Nanocage Hybrid Nanostructures as High-Performance Catalysts for Cascade Reactions. *Small* **2019**, *15*, e1903182.
- 101. Nazemi, M.; El-Sayed, M. A. The Role of Oxidation of Silver in Bimetallic Gold-Silver Nanocages on Electrocatalytic Activity of Nitrogen Reduction Reaction. *J. Phys. Chem. C* **2019**, *123*, 11422-11427.
- 102. Fan, X.; Zheng, W.; Singh, D. J. Light Scattering and Surface Plasmons on Small Spherical Particles. *Light: Sci. Appl.* **2014**, *3*, e179.
- 103. Le-Van, Q.; Zoethout, E.; Geluk, E. J.; Ramezani, M.; Berghuis, M.; Gómez Rivas, J. Enhanced Quality Factors of Surface Lattice Resonances in Plasmonic Arrays of Nanoparticles. *Adv. Opt. Mater.* **2019**, *7*, 1801451.
- 104. Wang, L.; Hasanzadeh Kafshgari, M.; Meunier, M. Optical Properties and Applications of Plasmonic-Metal Nanoparticles. *Adv. Funct. Mater.* **2020**, *30*, 2005400.
- 105. Li, J.-M.; Yang, Y.; Qin, D. Hollow nanocubes made of Ag-Au alloys for SERS detection

- with sensitivity of  $10^{-8}$  M for melamine. J. Mater. Chem. C 2014, 2, 9934-9940.
- 106. Ye, H.; Xia, X. Enhancing the Sensitivity of Colorimetric Lateral Flow Assay (CLFA) through Signal Amplification Techniques. *J. Mater. Chem. B* **2018**, *6*, 7102-7111.
- 107. Love, J. C.; Estroff, L. A.; Kriebel, J. K.; Nuzzo, R. G.; Whitesides, G. M. Self-Assembled Monolayers of Thiolates on Metals as a Form of Nanotechnology. *Chem. Rev.* **2005**, *105*, 1103-1170.
- 108. Glomm, W. R.; Halskau, Ø.; Hanneseth, A.-M. D.; Volden, S. Adsorption Behavior of Acidic and Basic Proteins onto Citrate-Coated Au Surfaces Correlated to Their Native Fold, Stability, and pl. J. Phys. Chem. B 2007, 111, 14329-14345.
- 109. Ha, M.; Kim, J. H.; You, M.; Li, Q.; Fan, C.; Nam, J. M. Multicomponent Plasmonic Nanoparticles: From Heterostructured Nanoparticles to Colloidal Composite Nanostructures. *Chem. Rev.* **2019**, *119*, 12208-12278.
- 110. Lindley, S. A.; Cooper, J. K.; Rojas-Andrade, M. D.; Fung, V.; Leahy, C. J.; Chen, S.; Zhang, J. Z. Highly Tunable Hollow Gold Nanospheres: Gaining Size Control and Uniform Galvanic Exchange of Sacrificial Cobalt Boride Scaffolds. ACS Appl. Mater. Interfaces 2018, 10, 12992-13001.
- 111. Chen, B. B.; Liu, M. L.; Zou, H. Y.; Liu, Y.; Li, Y. F.; Swihart, M. T.; Huang, C. Z. *In Situ* Imaging of Ion Motion in a Single Nanoparticle: Structural Transformations in Selenium Nanoparticles. *Angew. Chem.* **2022**, *61*, e202210313.
- 112. Cheng, H.; Wang, C.; Lyu, Z.; Zhu, Z.; Xia, Y. Controlling the Nucleation and Growth of Au on *a*-Se Nanospheres to Enhance Their Cellular Uptake and Cytotoxicity. *J. Am. Chem. Soc.* **2023**, *145*, 1216-1226.
- 113. Cai, K.; Zhang, W.; Foda, M. F.; Li, X.; Zhang, J.; Zhong, Y.; Liang, H.; Li, H.; Han, H.; Zhai, T. Miniature Hollow Gold Nanorods with Enhanced Effect for *In Vivo* Photoacoustic Imaging in the NIR-II Window. *Small* **2020**, *16*, e2002748.
- 114. Shao, S.; Wang, A.; Gupta, R.; Zou, S.; Xia, X. On the Role of Wall Thickness in Determining the Plasmonic Properties of Silver-Gold Nanocages. *Chem. Commun.* **2023**, *59*, 8059-8062.
- 115. Hood, Z. D.; Kubelick, K. P.; Gilroy, K. D.; Vanderlaan, D.; Yang, X.; Yang, M.; Chi, M.; Emelianov, S. Y.; Xia, Y. Photothermal Transformation of Au-Ag Nanocages under Pulsed Laser Irradiation. *Nanoscale* **2019**, *11*, 3013-3020.
- 116. Link, S.; Burda, C.; Nikoobakht, B.; El-Sayed, M. A. Laser-Induced Shape Changes of

- Colloidal Gold Nanorods Using Femtosecond and Nanosecond Laser Pulses. *J. Phys. Chem. B* **2000**, *104*, 6152-6163.
- 117. Huang, X.; El-Sayed, I. H.; Qian, W.; El-Sayed, M. A. Cancer Cell Imaging and Photothermal Therapy in the Near-Infrared Region by Using Gold Nanorods. *J. Am. Chem. Soc.* **2006**, *128*, 2115-2120.
- 118. Shao, S.; Zhu, X.; Ten, V.; Kim, M. J.; Xia, X. Understanding the Impact of Wall Thickness on Thermal Stability of Silver-Gold Nanocages. *J. Phys. Chem. C* **2022**, *126*, 7337-7345.
- 119. Olson, T. Y.; Schwartzberg, A. M.; Orme, C. A.; Talley, C. E.; O'Connell, B.; Zhang, J. Z. Hollow Gold-Silver Double-Shell Nanospheres: Structure, Optical Absorption, and Surface-Enhanced Raman Scattering. *J. Phys. Chem. C* 2008, *112*, 6319-6329.
- 120. Sun, Y.; Wiley, B.; Li, Z.-Y.; Xia, Y. Synthesis and Optical Properties of Nanorattles and Multiple-Walled Nanoshells/Nanotubes Made of Metal Alloys. *J. Am. Chem. Soc.* **2004**, *126*, 9399-9406.
- 121. Yu, L.; Hu, H.; Wu, H. B.; Lou, X. W. Complex Hollow Nanostructures: Synthesis and Energy-Related Applications. *Adv. Mater.* **2017**, *29*, 1604563.
- 122. Sun, Y.; Xia, Y. Multiple-Walled Nanotubes Made of Metals. Adv. Mater. 2004, 16, 264-268.
- 123. Sena-Torralba, A.; Álvarez-Diduk, R.; Parolo, C.; Piper, A.; Merkoçi, A. Toward Next Generation Lateral Flow Assays: Integration of Nanomaterials. *Chem. Rev.* **2022**, *122*, 14881-14910.
- 124. Khelifa, L.; Hu, Y.; Jiang, N.; Yetisen, A. K. Lateral Flow Assays for Hormone Detection. *Lab Chip* **2022**, *22*, 2451-2475.
- 125. Posthuma-Trumpie, G. A.; Korf, J.; van Amerongen, A. Lateral Flow (Immuno)assay: its Strengths, Weaknesses, Opportunities and Threats. A Literature Survey. *Anal. Bioanal. Chem.* **2009**, *393*, 569-582.
- 126. Quesada-González, D.; Merkoçi, A. Nanoparticle-based Lateral Flow Biosensors. *Biosens. Bioelectron.* **2015**, *73*, 47-63.
- 127. Zhou, W.; Gao, X.; Liu, D.; Chen, X. Gold Nanoparticles for *In Vitro* Diagnostics. *Chem. Rev.* **2015**, *115*, 10575-10636.
- 128. Glynou, K.; Ioannou, P. C.; Christopoulos, T. K.; Syriopoulou, V. Oligonucleotide-Functionalized Gold Nanoparticles as Probes in a Dry-Reagent Strip Biosensor for DNA Analysis by Hybridization. *Anal. Chem.* **2003**, *75*, 4155-4160.

- 129. Wei, Z.; Luciano, K.; Xia, X. Catalytic Gold-Iridium Nanoparticles as Labels for Sensitive Colorimetric Lateral Flow Assay. *ACS Nano* **2022**, *16*, 21609-21617.
- 130. Gao, Z.; Ye, H.; Tang, D.; Tao, J.; Habibi, S.; Minerick, A.; Tang, D.; Xia, X. Platinum-Decorated Gold Nanoparticles with Dual Functionalities for Ultrasensitive Colorimetric *In Vitro* Diagnostics. *Nano Lett.* **2017**, *17*, 5572-5579.
- 131. Faunce, T.; Styring, S.; Wasielewski, M. R.; Brudvig, G. W.; Rutherford, A. W.; Messinger, J.; Lee, A. F.; Hill, C. L.; deGroot, H.; Fontecave, M.; et al. Artificial Photosynthesis as a Frontier Technology for Energy Sustainability. *Energy Environ. Sci.* **2013**, *6*, 1074-1076.
- 132. Wang, P.; Huang, B.; Lou, Z.; Zhang, X.; Qin, X.; Dai, Y.; Zheng, Z.; Wang, X. Synthesis of Highly Efficient Ag@AgCl Plasmonic Photocatalysts with Various Structures. *Chem. Eur. J.* **2010**, *16*, 538-544.
- 133. Xiang, Q.; Yu, J.; Cheng, B.; Ong, H. C. Microwave-Hydrothermal Preparation and Visible-Light Photoactivity of Plasmonic Photocatalyst Ag-TiO<sub>2</sub> Nanocomposite Hollow Spheres. *Chem.: Asian J.* **2010**, *5*, 1466-1474.
- 134. Qi, J.; Lai, X.; Wang, J.; Tang, H.; Ren, H.; Yang, Y.; Jin, Q.; Zhang, L.; Yu, R.; Ma, G.; et al. Multi-Shelled Hollow Micro-/Nanostructures. *Chem. Soc. Rev.* **2015**, *44*, 6749-6773.
- 135. Mukherjee, S.; Ramalingam, B.; Griggs, L.; Hamm, S.; Baker, G. A.; Fraundorf, P.; Sengupta, S.; Gangopadhyay, S. Ultrafine Sputter-Deposited Pt Nanoparticles for Triiodide Reduction in Dye-Sensitized Solar Cells: Impact of Nanoparticle Size, Crystallinity and Surface Coverage on Catalytic Activity. *Nanotechnology* 2012, 23, 485405.
- 136. Li, Y.; Yu, Y.; Huang, Y.; Nielsen, R. A.; Goddard, W. A., III; Li, Y.; Cao, L. Engineering the Composition and Crystallinity of Molybdenum Sulfide for High-Performance Electrocatalytic Hydrogen Evolution. *ACS Catal.* **2015**, *5*, 448-455.
- 137. Lu, N.; Wang, J.; Xie, S.; Xia, Y.; Kim, M. J. Enhanced Shape Stability of Pd-Rh Core-Frame Nanocubes at Elevated Temperature: *In Situ* Heating Transmission Electron Microscopy. *Chem. Commun.* **2013**, *49*, 11806-11808.
- 138. Pawlik, V. D.; Zhao, X.; Figueras-Valls, M.; Wolter, T. J.; Hood, Z. D.; Ding, Y.; Liu, J.; Chi, M.; Mavrikakis, M.; Xia, Y. Thermal Stability of Au Rhombic Dodecahedral Nanocrystals Can Be Greatly Enhanced by Coating Their Surface with an Ultrathin Shell of Pt. *Nano Lett.* 2024, 24, 549-556.
- 139. Zhao, M.; Chen, Z.; Lyu, Z.; Hood, Z. D.; Xie, M.; Vara, M.; Chi, M.; Xia, Y. Ru Octahedral

- Nanocrystals with a Face-Centered Cubic Structure, {111} Facets, Thermal Stability up to 400 °C, and Enhanced Catalytic Activity. *J. Am. Chem. Soc.* **2019**, *141*, 7028-7036.
- 140. Vara, M.; Wang, X.; Howe, J.; Chi, M.; Xia, Y. Understanding the Stability of Pt-Based Nanocages under Thermal Stress Using *In Situ* Electron Microscopy. *ChemNanoMat* **2017**, *4*, 112-117.
- 141. Vara, M.; Roling, L. T.; Wang, X.; Elnabawy, A. O.; Hood, Z. D.; Chi, M.; Mavrikakis, M.; Xia, Y. Understanding the Thermal Stability of Palladium-Platinum Core-Shell Nanocrystals by *In Situ* Transmission Electron Microscopy and Density Functional Theory. *ACS Nano* **2017**, *11*, 4571-4581.
- 142. Zhang, L.; Xia, Y. Scaling up the Production of Colloidal Nanocrystals: Should We Increase or Decrease the Reaction Volume? *Adv. Mater.* **2014**, *26*, 2600-2606.
- 143. Mohammadi, M. M.; Gunturi, S. S.; Shao, S.; Konda, S.; Buchner, R. D.; Swihart, M. T. Flame-Synthesized Nickel-Silver Nanoparticle Inks Provide High Conductivity without Sintering. *Chem. Eng. J.* **2019**, *372*, 648-655.
- 144. Kumar, D. V. R.; Kasture, M.; Prabhune, A. A.; Ramana, C. V.; Prasad, B. L. V.; Kulkarni, A. A. Continuous Flow Synthesis of Functionalized Silver Nanoparticles using Bifunctional Biosurfactants. *Green Chem.* **2010**, *12*, 609-615.
- 145. Mohammadi, M. M.; Shao, S.; Srivatsa Gunturi, S.; Raghavan, A. R.; Alexander, N.; Liu, Y.; Stafford, C. M.; Buchner, R. D.; Swihart, M. T. A General Approach to Multicomponent Metal-Decorated Crumpled Reduced Graphene Oxide Nanocomposites Using a Flame-based Process. *Nanoscale* **2019**, *11*, 19571-19578.

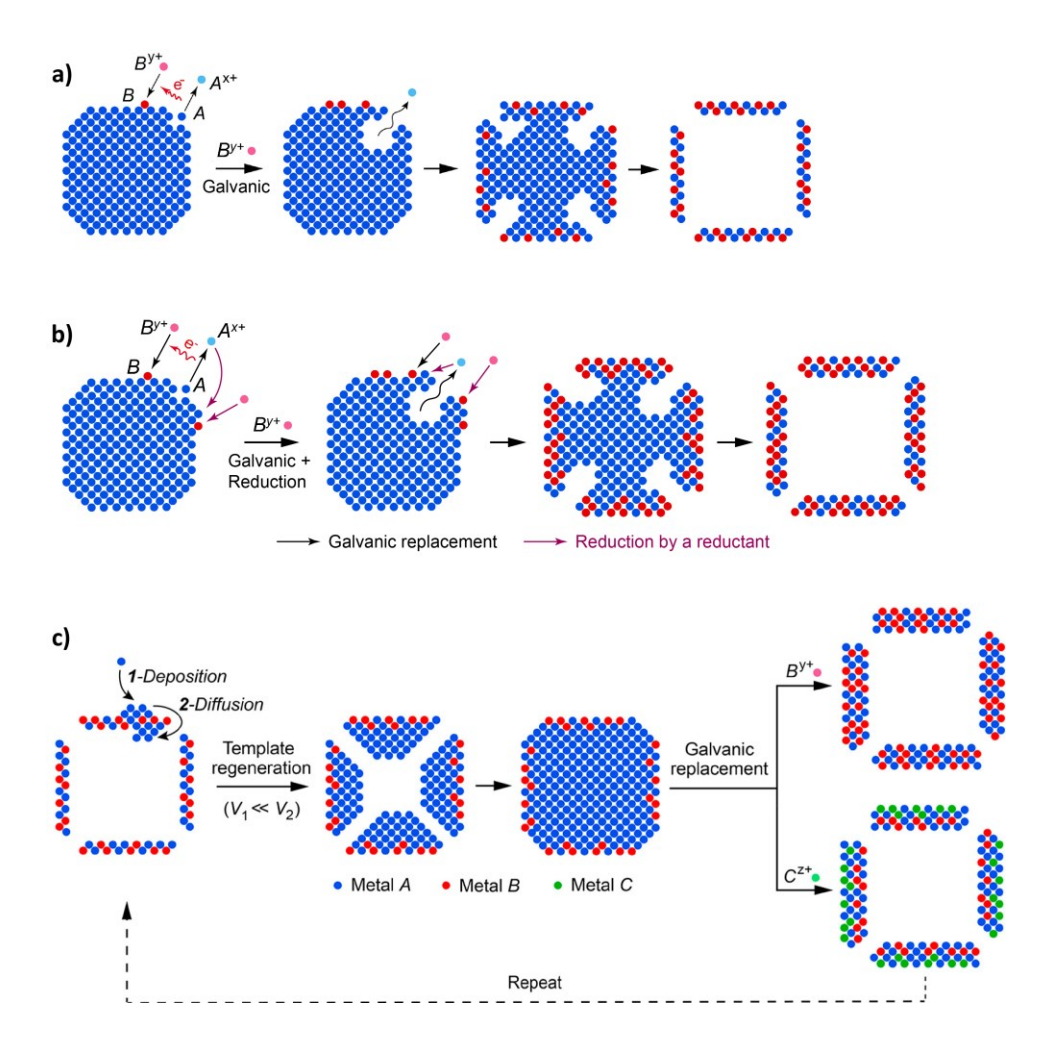


**Figure 1.** Schematics showing different galvanic replacement reaction (GRR)-based methods for the synthesis of plasmonic hollow nanostructures. a) conventional GRR between template of metal A with ions of metal B ( $B^{y+}$ ), which generates A-B alloyed nanocage; b) the coupling of GRR with co-reduction; and c) the coupling of GRR with template regeneration. a) and c) are adapted with permission from ref 2. Copyright 2020 American Chemical Society.

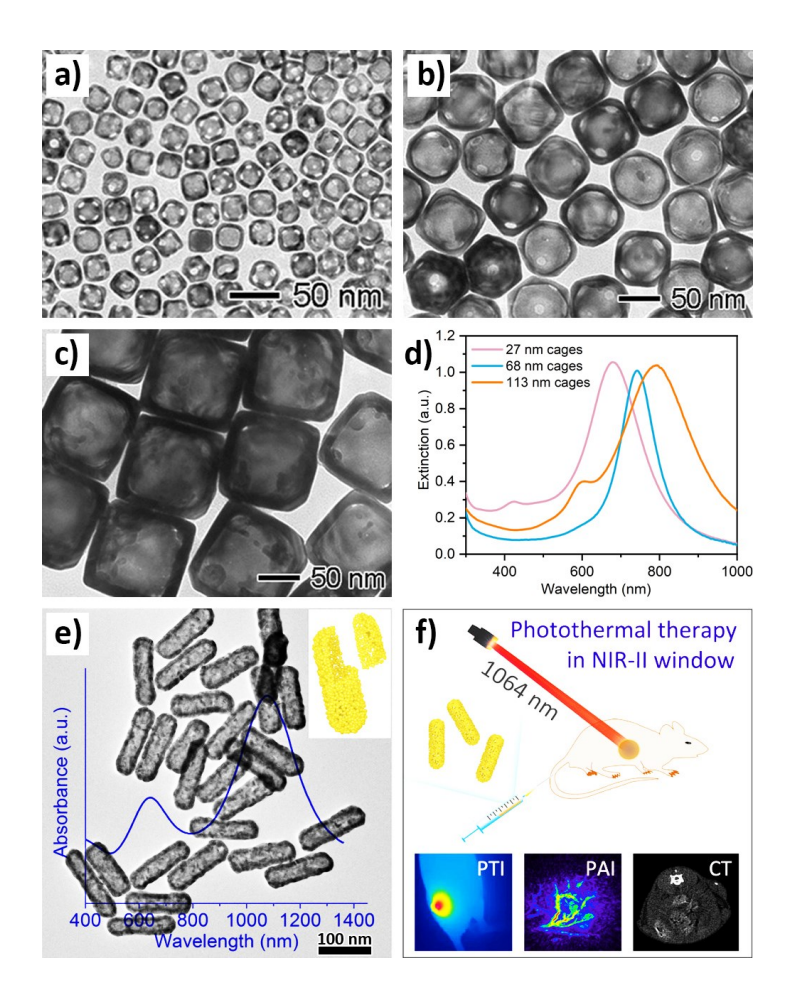


**Figure 2.** Plasmonic hollow nanostructures with different void morphologies (*i.e.*, size and shape). a-c) Transmission electron microscopy (TEM) images of a) 27 nm, b) 68 nm, and c) 113 nm Ag-Au nanocages; d) Corresponding LSPR extinction spectra recorded from the samples in a-c); e) TEM image and UV-vis-NIR spectrum of a typical Au hollow nanorod sample. The 100 nm scale bar applies to the TEM image; f) Application of the Au hollow nanorods in biomedical imaging and therapy. a-d) are adapted with permission from ref 1. Copyright 2021 American Chemical Society. e, f) are adapted with permission from ref 97. Copyright 2018 American Chemical Society.

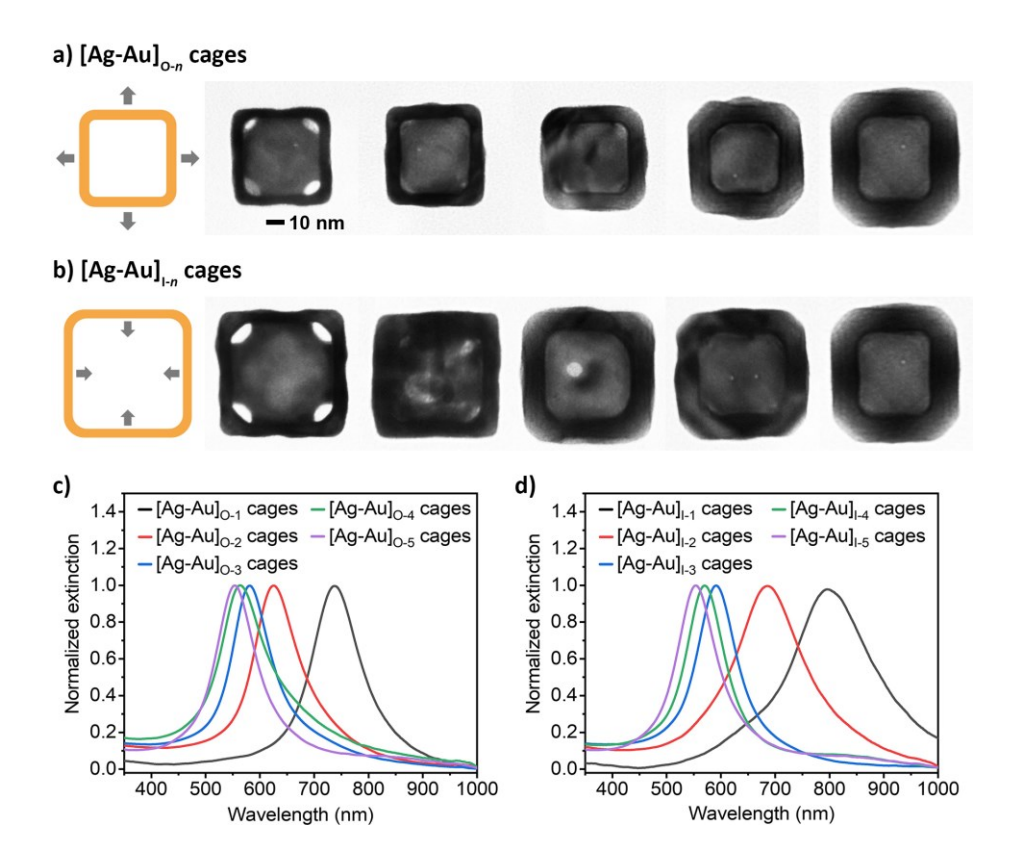
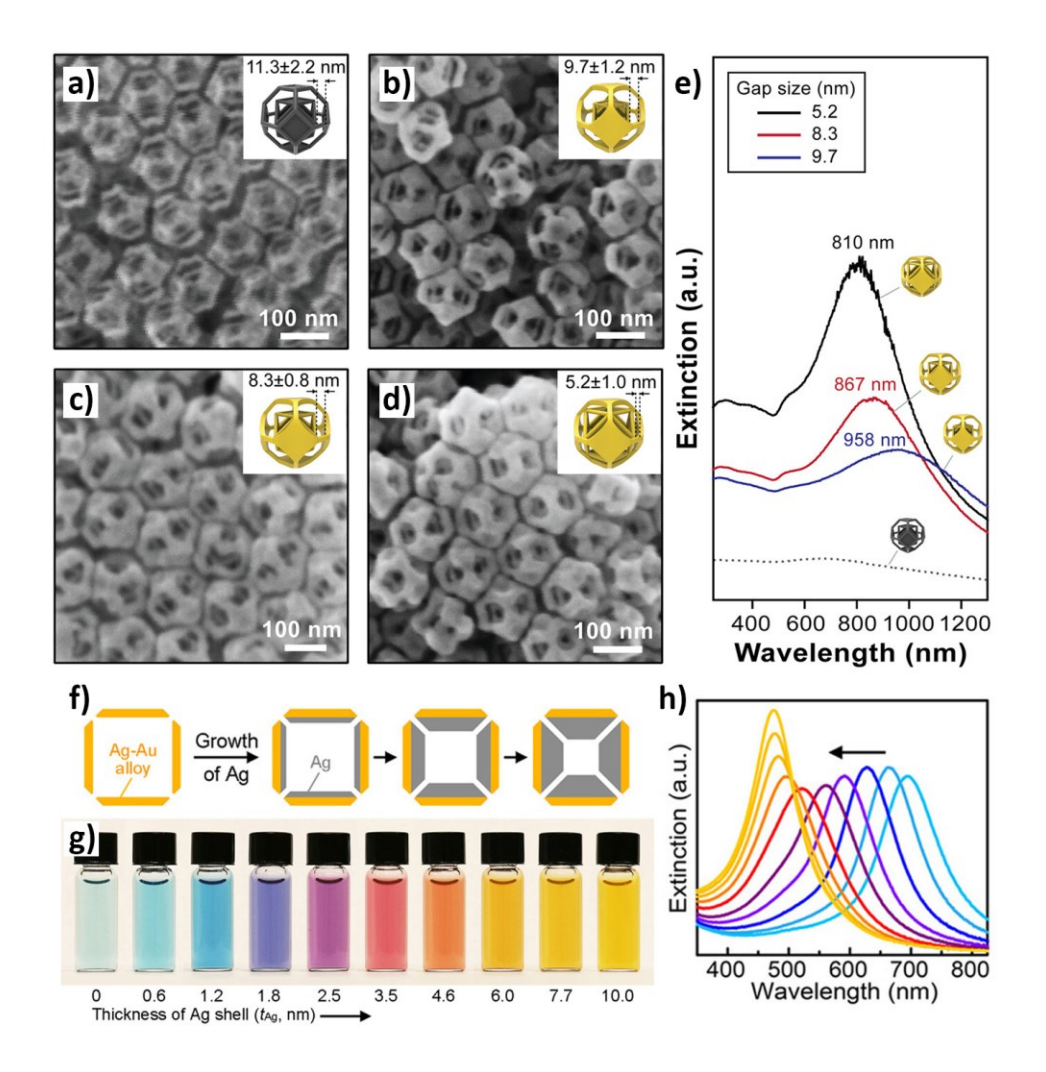
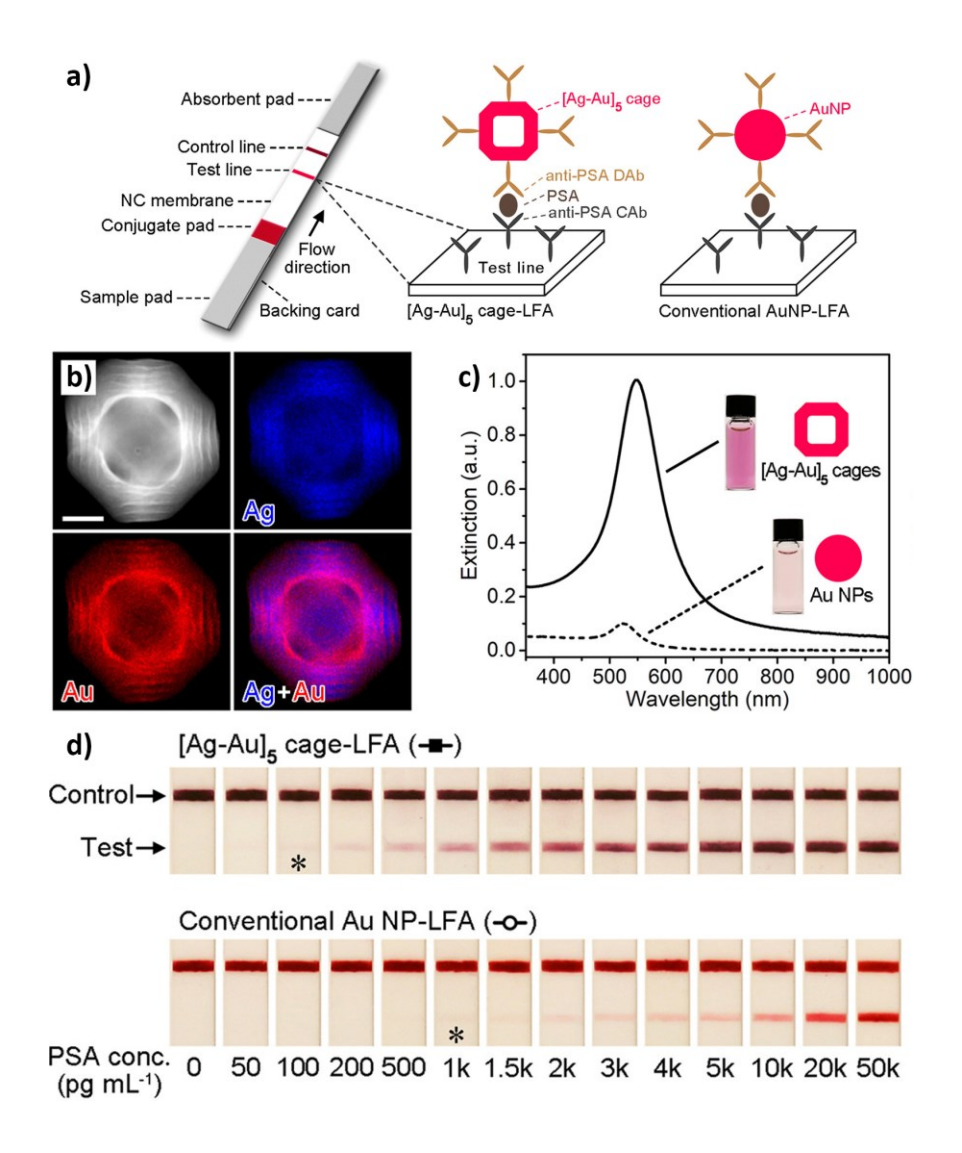


Figure 3. Ag-Au nanocages with different wall thicknesses. a) A schematic and corresponding TEM images of individual [Ag-Au]o-n cages. As indicated by the arrows in the schematic, the wall thickness increases toward outer surface of the cage while the internal void size remains unchanged; b) A schematic and corresponding TEM images of individual [Ag-Au]<sub>I-n</sub> cages. The wall thickness increases toward inner surface of the cage while the outer diameter remains unchanged; c) Normalized LSPR peaks corresponding to the samples in a); d) Normalized LSPR peaks corresponding to the samples in b). The scale bar in a) applies to all TEM images. Adapted with permission from ref 114. Copyright 2023 The Royal Society of Chemistry.



**Figure 4.** Plasmonic hollow nanostructures with various inner shells. a-d) Field-emission scanning electron microscopy (FE-SEM) images of a) Pt nanoframe, and b-d) Au double-walled nanoframes with two face-to-face segregated walls; e) Corresponding UV-vis-NIR spectra of samples in a-d). f) Schematics showing the growth of consecutive Ag shells on the inner surfaces of preformed Ag-Au nanocages, forming Ag@Ag-Au shell@shell cages; g) Photographs taken from aqueous suspensions of Ag@Ag-Au cages with different inner Ag shell thicknesses in the range of 0-10.0 nm; h) Corresponding UV-vis spectra recorded from the samples in g). a-e) are reprinted with permission from ref 60. Copyright 2023 American Chemical Society. f-h) are reprinted with permission from ref 1. Copyright 2021 American Chemical Society.



**Figure 5.** Application of Ag-Au nanocages in lateral flow assay (LFA). a) Principles of LFAs for PSA detection using Ag-Au nanocages with five consecutive Ag-Au alloyed layers in the wall ([Ag-Au]<sub>5</sub> cages) and Au NPs as labels, respectively; b) Energy-dispersive X-ray (EDX) mapping images of an individual [Ag-Au]<sub>5</sub> cage; c) LSPR spectra comparing the extinction intensities of the [Ag-Au]<sub>5</sub> cages and 40 nm Au NPs at the same particle concentration; d) Representative photographs taken from the [Ag-Au]<sub>5</sub> cage- and Au NP-based LFAs for PSA standards. The asterisks (\*) indicate the detection limits by the naked eyes. Adapted with permission from ref 2. Copyright 2020 American Chemical Society.

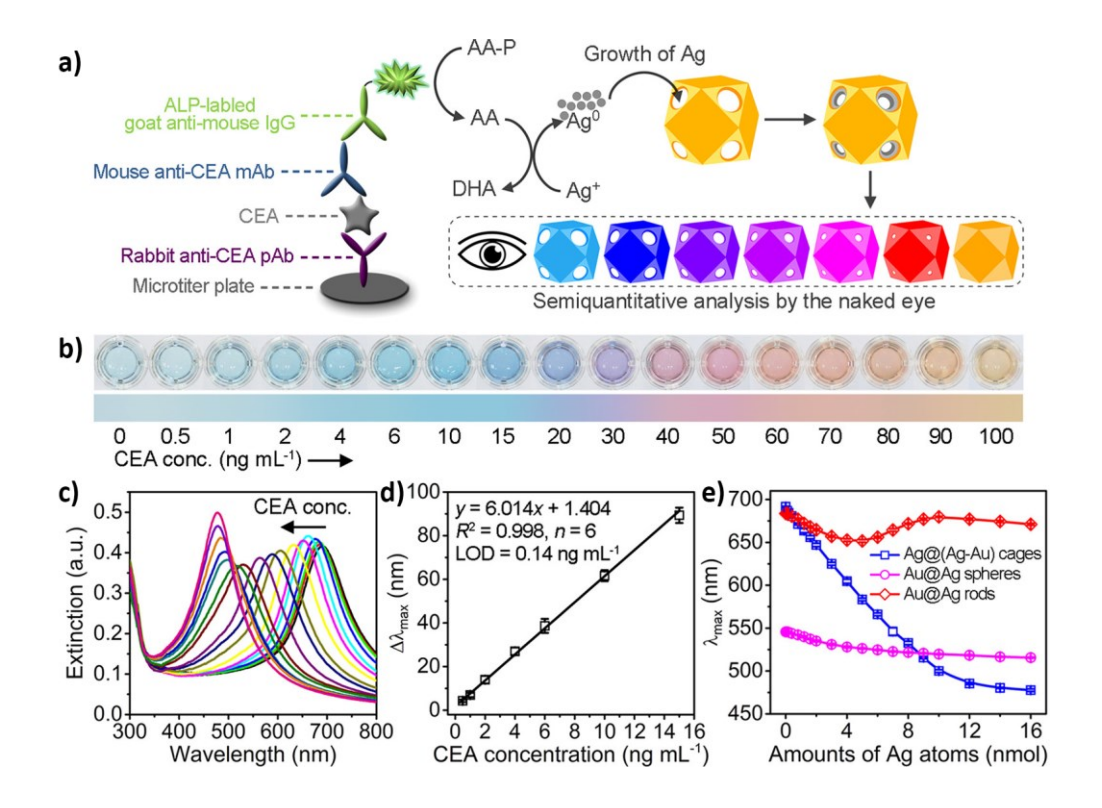


**Figure 6.** A biosensing platform based on Ag@Ag-Au shell@shell nanocages for detection of CEA. a) Schematics showing the detection principle. ALP: alkaline phosphatase; AA-P: L-ascorbic acid 2-phosphate; DHA: L-dehydroascorbic acid; b) Representative photographs taken from the detection results of CEA standards; c) LSPR extinction spectra of the solution shown in b); d) Linear range region of the biosensing system. Error bars indicate the standard deviations (n = 6); e) Comparison of major LSPR peaks ( $\lambda_{max}$ ) of different nanocrystals that were prepared by depositing the same amount of Ag atoms on preformed hollow Ag-Au nanocages (blue; note, Ag was deposited on inner surfaces), solid Au nanospheres (magenta), and solid Au nanorods (red). Reprinted with permission from ref 1. Copyright 2021 American Chemical Society.

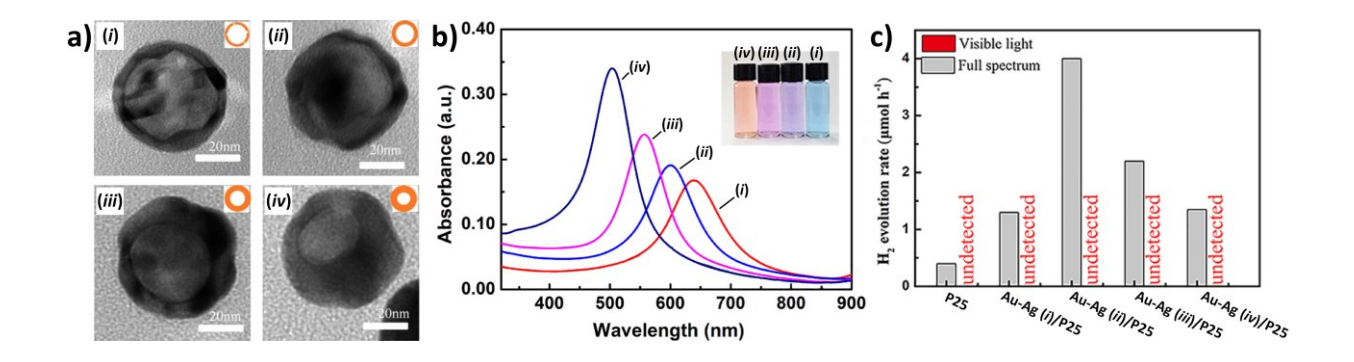


**Figure 7.** Application of Au-Ag hollow nanoparticles (HNPs) in photocatalysis for H<sub>2</sub> evolution. a) TEM images of four different Au-Ag HNPs with void sizes in the descending order of (*i*), (*ii*), (*iii*), and (*iv*); b) UV-vis spectra and photographs taken from the samples in a); c) Photocatalytic H<sub>2</sub> evolution rates in 25 vol% methanol for pure P25 TiO<sub>2</sub> and Au-Ag HNPs/P25 composites under full spectrum and visible light irradiations. Adapted with permission from ref 69. Copyright 2020 Elsevier.